Phys Chem Minerals (2010) 37:291–300
DOI 10.1007/s00269-009-0333-z

ORIGINAL PAPER

Synthetic *near* Σ5 (210)/[100] grain boundary in YAG fabricated by direct bonding: structure and stability

Katharina Hartmann · Richard Wirth · Wilhelm Heinrich

Received: 24 July 2009 / Accepted: 29 September 2009 / Published online: 22 October 2009

Abstract Several macroscopic physical and chemical properties, such as rheology, elasticity, or transport properties are governed by grain boundary processes. An improved understanding of the structure and evolution of grain boundaries has thus become a key challenge in geosciences and material sciences. Here, we report the structure of *near* Σ5 (210)/[100] grain boundaries in $Y_3Al_5O_{12}$ (YAG), which were synthesised by the wafer direct bonding method. The produced grain boundaries were annealed at different temperatures, ranging from 673 to 1,873 K. The grain boundaries annealed at different temperatures are not distinguishable based on their flatness and apparent cohesiveness in high resolution TEM (HRTEM) micrographs, but show a considerable step in their mechanical stability at around 1,273 K, a temperature that corresponds to roughly half the melting temperature of YAG. This study further focuses on the effect of a slight misorientation of the two crystals on the grain boundary structure and we discuss if the boundary can reach a state of minimum energy configuration during annealing. Along the grain boundaries, we observed a long-range strain contrast with a periodicity of 40 nm, which has not been reported for high-angle grain boundaries so far. We conclude that this contrast is caused by faceting along the grain boundary plane, which is needed to achieve minimum energy configuration of the grain boundary plane.

Keywords Grain boundary · Structure · TEM · FIB · Sigma relation · CSL · Garnet · Wafer bonding · Long-range strain contrast

K. Hartmann (✉) · R. Wirth · W. Heinrich
German Research Centre for Geosciences GFZ, Sect. 3.3, 14473 Potsdam, Germany
e-mail: Hartmann@gfz-potsdam.de

Introduction

Our current understanding of grain boundaries mainly emerged from studies on metals and alloys (Gleiter and Chalmers 1972; Carter and Föll 1978; Föll and Ast 1979; Carter et al. 1981; Cunningham et al. 1982; Sutton and Balluffi 1995; Christophersen et al. 2001; Merkle et al. 2004; Randle et al. 2008). Beyond that, grain boundaries in complex ionic compounds, such as ceramics, have been studied extensively starting in the early 1980s till now (Ernst et al. 1999; Lee et al. 2003b). Despite their importance for our understanding of several physical and chemical properties, for instance rheology, elasticity, or transport properties, grain boundary studies are still rare in earth sciences (e.g. Bons et al. 1990; Keller et al. 2008). During the last decades element transport in natural materials has been brought in the focus of mineral and geosciences (Jaoul et al. 1991; Joesten 1991; Abart et al. 2004, 2009; Milke et al. 2009; Schmid et al. 2009). Understanding and measuring element diffusion along single grain boundaries has become a key challenge. This increasing interest motivates our aim to produce well characterisable grain boundaries over mm ranges.

It can be an expensive and time-consuming challenge to produce long-range interfaces with constant characteristics, for example using ultra high vacuum (UHV) bonding (Kim and Carpenter 2002; Gemming et al. 2003; Razek et al. 2007). However, wafer direct bonding, also termed 'direct bonding' or 'fusion bonding', is a method to join two well polished material slices without glue, force, or UHV at ambient conditions (Harendt et al. 1992; Pößl and Kräuter 1999). The method is relatively simple and does not require sophisticated or expensive machines. It can be applied to most materials (Haisma et al. 1994; Tong et al. 1995; Tong and Gösele 1999) and allows the production of any desired

grain boundary orientation with an accuracy of about 0.5°. The bonding that is achieved at ambient conditions is relatively weak in comparison to metallic, covalent or ionic interactions in the volume of the crystals, but it strengthens during heating. Therefore, annealing at elevated temperatures is favourable for many applications. The interface strength depends on the surface energies and the bond strengths and it is generally quantified by crack-opening (Gösele et al. 1999).

In the past, the direct wafer bonding method was mainly applied to semiconductors or electronic devices (Maszara 1991; Harendt et al. 1992; Tong and Gösele 1999), but has recently been adopted to geo-materials (Haisma et al. 1994; Heinemann et al. 2001, 2003, 2005). Heinemann et al. (2005) observed that synthetic grain boundaries in forsterite (Mg_2SiO_4) bicrystals formed after annealing for 7 days at 673 K. At the scale of HRTEM, the grain boundary region was fully crystalline and no evidence for amorphous material at the grain boundary was reported. Further annealing for 48 h at 1,923 K did not significantly change the grain boundary structure. So far, it is not fully understood at which temperatures the grain boundary achieves its maximum stability and if a random grain boundary is able to reach a minimum energy configuration during long annealing periods.

To address these questions, we synthesised a *near* Σ5 (210)/[100] grain boundary in yttrium aluminium garnet (YAG) by using the direct wafer bonding method at different annealing temperatures. YAG bicrystals with a perfect Σ5 (210)/[100] grain boundary have previously been synthesised using the UHV method (Campbell 1996), which serves as a useful reference for this study.

Garnets crystallize in the highest symmetric space group *Ia3d* of the cubic crystal system (bcc). In $Y_3Al_2Al_3O_{12}$ (YAG), yttrium occupies the large dodecahedral positions exclusively, whereas the aluminium is distributed between the octahedral and tetrahedral sites. The unit cell consists of 160 atoms corresponding to eight formula units (Kuklja and Pandey 1999; Dobrzycki et al. 2004). It has an extremely high melting point of 2,213 K (Caslavsky and Viechnicki 1980) and is perfectly suited for this study because large stoichiometric crystals of high quality can be synthesised and polishing techniques have been adapted to YAG as it is used for many technological applications, such as solid state lasers. Furthermore, YAG is highly stable under the electron beam, which is prerequisite for extended exposure times to the electron beam during zone axis alignment to obtain high quality HRTEM images.

In this study, we monitor the relation between final boundary strength and annealing temperature in order to better constrain the required minimum annealing temperature that leads to a stable interface. Furthermore, we address the effect of a slight misorientation of the two crystals on the grain boundary structure and we test if the boundary reaches a state of minimum energy configuration during annealing.

Grain boundary models

A minimum of five parameters, consisting of three Miller indices for the grain boundary plane <hkl> in the reference crystal and two rotational angles to describe the orientations of the respective grains, is required to fully describe a grain boundary. Alternatively, one angle and two sets of Miller indices (one that represents the grain boundary plane and one that gives the direction of the axis of the rotation) can be used. Most commonly, grain boundaries and crystal to crystal orientations are described by the coincidence site model (Gleiter and Chalmers 1972; Chadwick and Smith 1976; Sutton and Balluffi 1995). In this model, two–three-dimensional lattices are super-imposed and translated until they coincide at lattice sites (Fig. 1) and thereby generate a super periodicity or 'super lattice', which is referred to as the coincidence site lattice (CSL). The Σ-nomenclature is commonly used to describe the relation between the number of lattice points in the unit cell of a CSL and the number of lattice points in the unit cells of the generating lattices and is defined as:

$$\Sigma = 1/n$$

where n is the fraction of the lattice points of the two superimposed lattices that coincide.

We emphasize that the Σ relation does exclusively define the crystal to crystal orientation. But two grains displaying a Σ-relation may be joined by a grain boundary plane with high energy. For each specific CSL, high interface coincidences and thus energetic minima only exist for certain grain boundary plane orientations which are likely to occur at the closest packed planes of the corresponding CSL (Rohrer et al. 2004; Rohrer 2007).

A grain boundary that is not exactly at the plane of highest coincidence site density can reduce its energy by faceting. This can be achieved with or without inserting secondary grain boundary dislocations, but in both cases the total boundary area increases [Fig. 1c, see also Brandon (1966)]. Faceting requires movements of atoms over short distances and thus sufficiently high temperatures. For the total free energy of a polycrystal, the grain boundary plane is of minor importance compared to the relative orientation of all the crystals towards each other.

Based on theoretical arguments, it is expected that two crystals that are close to a low energy crystal orientation relation will minimize their grain boundary energy by turning into a Σ-relation, which generally has low energy. However, this would require a movement of all the atoms inside one grain. Alternatively, the small misorientation

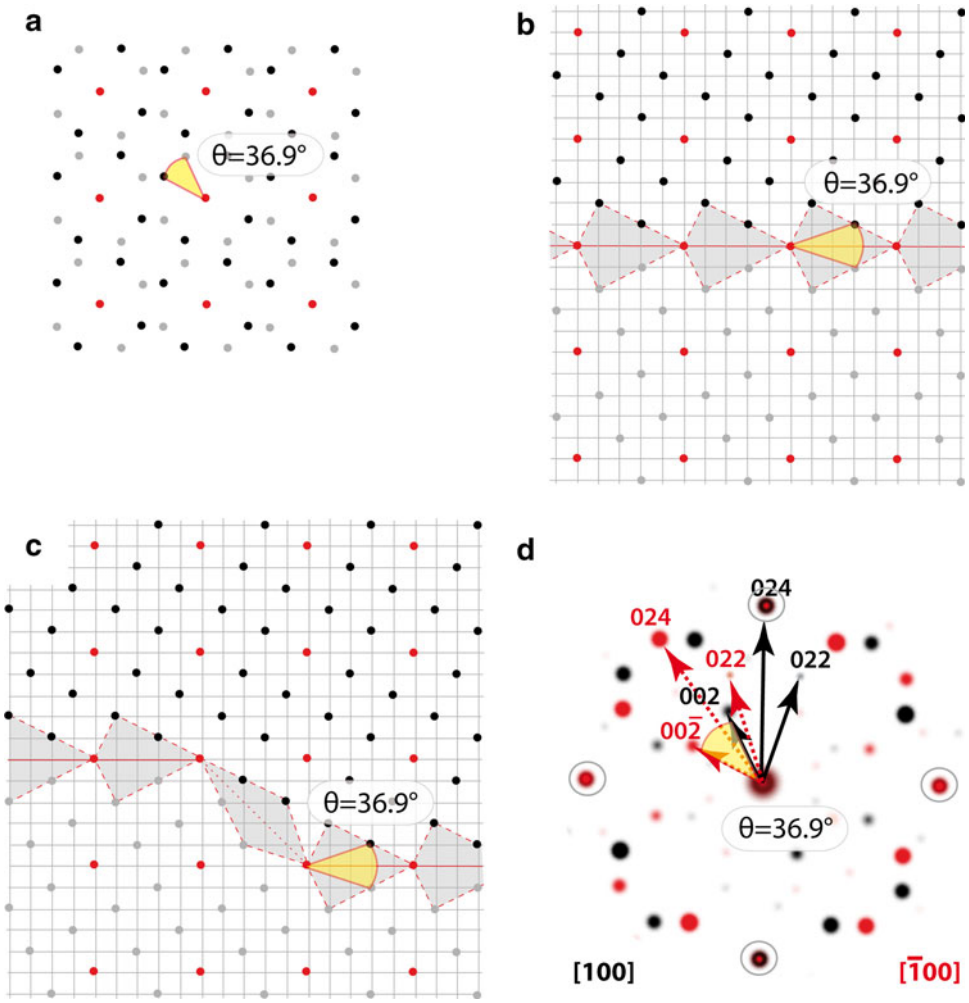

Fig. 1 Sketch of the coincidence site lattice (*CSL*). **a** The example shows the CSL (*red*) of a Σ5 coincidence site lattice that is produced by superimposing two lattices (*grey* and *black*) with a misorientation angle θ of 36.9°. **b** Sketch of a geometrical Σ5 (210)/[100] grain boundary, which is a twin about the (210) plane. The tilt of $\theta = 36.9°$ about the common [100] direction is structurally equal to a twist boundary of 180° parallel to the (210) plane. **c** Same grain boundary plane as in **b**, but faceted. No strain is generated as the step is between coincidence sites of the CSL. Additionally, the displacement shift complex (*DSC*) is indicated (*square lattice* in *grey colour*, see text for explanation). **d** Simulated diffraction pattern of the Σ5 (210)/[100] grain boundary. The coinciding diffraction spots are *circled*

could be overcome by superimposing a network of secondary dislocations to the present boundary, which is comparable to dislocations added to achieve the minimum energy grain boundary plane.

Methods

Bicrystal synthesis by direct bonding

YAG single crystal plates were mistilted by 3° parallel to the (210), which results in an angle of 93° between the [001] and our desired plane close to (210). Plates were cut and chemo-mechanically polished (CMP) with silica slurry. A KUGLER (KMS) interferometer was used for surface roughness measurements by determining the roughness average (Ra) values from the topography data of the computer-supported interference microscope. The final roughness of the crystal plates was about 0.34 nm.

The crystals were wet-chemically cleaned using a five step cleaning procedure in a clean room environment. In step one, a hydrogen per-oxide cleaning solution (pH ≈ 6.5) at 353 K was applied, the second step was a per-iodic acid cleaning to decompose organic adsorbants. In steps three and four, the crystal surfaces were cleaned with acetone and isopropanol, respectively. Finally, the surface is saturated with pure adsorbed water. In order to synthesize a bicrystal, an initial contact between two clean crystals was established by applying a slight pressure with tweezers. The initial bonding was further strengthened by heating in a vacuum furnace at 673 K and 10 Pa for 1 week. However, the achieved bond is mechanically easily separable. To increase the bonding strength additional annealing runs at 873, 1,073, 1,273, 1,473, 1,723 and 1,923 K for 48 h each were performed. A detailed description of the bonding method is given by Heinemann et al. (2001).

The Σ5 (210)/[100] grain boundary in cubic materials, is a tilt boundary of 36.9° about the bicrystals' common [100] direction, which is structurally equal to a twist boundary of 180° parallel to the (210) plane. The exact Σ5 (210)/[100] grain boundary has previously been synthesised in YAG

using the UHV-technique (Campbell 1996). In contrast, we produced a *near* Σ5 (210)/[100] grain boundary with direct bonding. We rotated the crystal wafers by 185° with a misfit of 3° to the (210) plane, thereby inducing an additional tilt of 6° between the [100] and the [$\bar{1}$00] direction. The results are shown in the lattice fringe images of Fig. 2. The optical isotropy of garnet prohibits a quantification of the orientation relation of the two crystals with optical microscopy. The misorientation of the two crystals with respect to the Σ5 (210)/[100] grain boundary is measured with an accuracy of about 0.1° with the TEM by using the alpha and beta tilts of the stage. First, the [100] direction of one crystal is aligned with the incident beam, followed by the [$\bar{1}$00] direction of the second crystal. The measured angle set is $\alpha = -2.86°$, $\beta = 1.43°$ and $\alpha = -2.52°$, $\beta = 8.08°$. The total misalignment between [100] and [$\bar{1}$00] direction is calculated by a rotational matrix conversion to be ~6.5° (±0.1°). Already short low temperature anneals bring the grain boundary plane parallel to the (210) plane.

Finally, we can fully describe the grain boundary as a *near* Σ5 (210)/[100] grain boundary, where the boundary plane lies in the (210) plane of both crystals. The rotation about the [100] direction is 36.9°, additionally, a rotation of 6.5° about the [210] direction is present.

Sample preparation

Lamellae for TEM ($15 \times 8 \times 0.1\ \mu m^3$) were prepared using the Focused Ion Beam (FIB) technique (Overwijk et al. 1993; Phaneuf 1999; Lee et al. 2003a; Wirth 2004). To obtain high quality HRTEM images, one sample was prepared at the application laboratory FEI Company, Eindhoven, Netherlands by using an in situ lift out method in the Helios Nanolab 600. A chunk of the material was removed from the bulk sample by using the FIB to remove material around it. The chunk was then transferred to the grid by attaching an Omniprobe to the lamella using FIB induced Pt deposition. Once attached to the grid, final thinning was performed on the lamella, initially at an acceleration voltage of 30 kV, and finally at 2 kV. Another lamella was prepared using a two-beam focused Ion beam (ZEISS NVision40 Argon) instrument with an implemented low energy Ar-ion gun (Penning Ion Gauge, PIG).

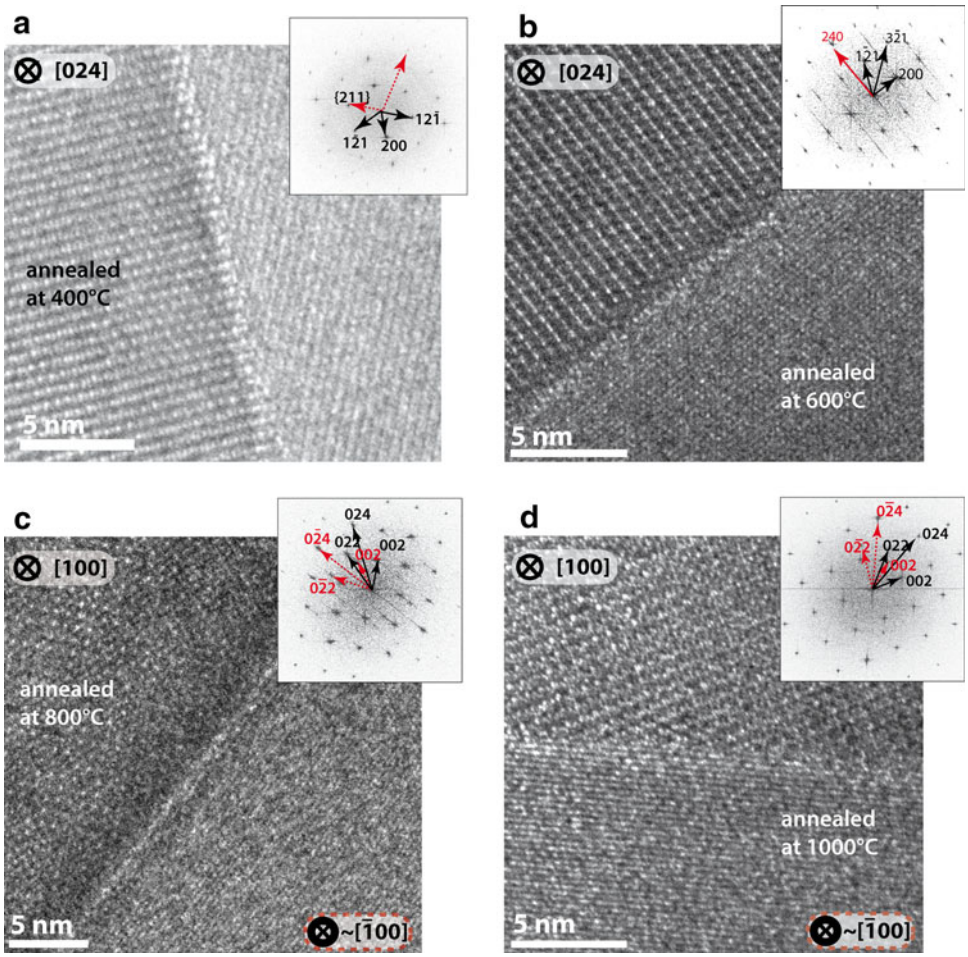

Fig. 2 Lattice fringe images of grain boundaries synthesized at 673, 873, 1,073 and 1,273 K (**a**–**d**). The grain boundaries bonded at 673, 873 and 1,073 K (**a**–**c**) can be easily separated mechanically, even though no apparent differences can be observed between their lattice fringe images and the one corresponding to the grain boundary synthesized at 1,273 K (**d**). At all stages, the lattice fringes of the opposing crystals touch each other at the interface and no amorphous material or material with different structures was observed. Images **a** and **c**, with a misorientation angle θ relative to the exact Σ5 (210)/[100] of ~8°, as well as **b** and **d** ($\theta \sim 6.5°$) have been taken along different zone axes because the bicrystals have slightly deviant orientations. The varying image quality results from the strongly differing thicknesses of the respective TEM lamellae

This method overcomes the problem of the amorphous layer forming during FIB sample preparation by Ga-ion implantation into the sample. Low voltage Ar-ion polishing with an acceleration voltage of 500 eV is suitable to remove the amorphous layer together with the implanted Ga from the FIB-lamellae surfaces.

TEM

A Tecnai F20 X-Twin TEM was operated at 200 kV acceleration voltage with a field emission gun (FEG) as electron source. The TEM is equipped with a post-column Gatan imaging filter (GIF Tridiem). All of the TEM images presented here are energy-filtered images applying a 10 eV window to the zero loss peak. The Gatan Digital Micrograph software was used for the analyses of the energy filtered transmission electron micrographs (EFTEM). The ring mask method was used for fast Fourier transform (FFT) analysis to prevent lattice fringe extrapolations (Pradère et al. 1988; Pradère and Thomas 1990).

Results

Bicrystal synthesis

The grain boundary formed by direct bonding is homogenous over a length of at least 10 μm. This minimum length is derived from TEM investigations of FIB-milled lamellae with the dimensions 15 × 10 μm^2. The grain boundaries that we annealed at different temperatures (673–1,873 K, Table 1) are not distinguishable based on their flatness and apparent cohesiveness (Fig. 2). However, the grain boundaries synthesized below 1,273 K are mechanically separable (compare Table 1 with Fig. 2). After annealing at 1,273 K or at higher temperature, bonding is strong enough that upon stress the bicrystals fracture at other locations than the interface. We also observed that the forsterite bicrystals synthesized at 673 K by Heinemann et al. 2005, which show comparable lattice fringe images, are mechanically separable as well.

Microstructure and orientation relation of the grain boundary

In the following, only the bicrystal synthesized at 1,273 K with a misorientation of 6.5° with respect to the perfect Σ5 (210)/[100] will be discussed. The grain boundary synthesized is thus a *near* Σ5 (210)/[100] grain boundary, as shown in the lattice fringe image of Fig. 3. The diffraction pattern (inset in Fig. 3) confirms the rotation of ~36.9° of the two crystals with respect to each other. The thinnest parts of the studied lamella showed a relative thickness of

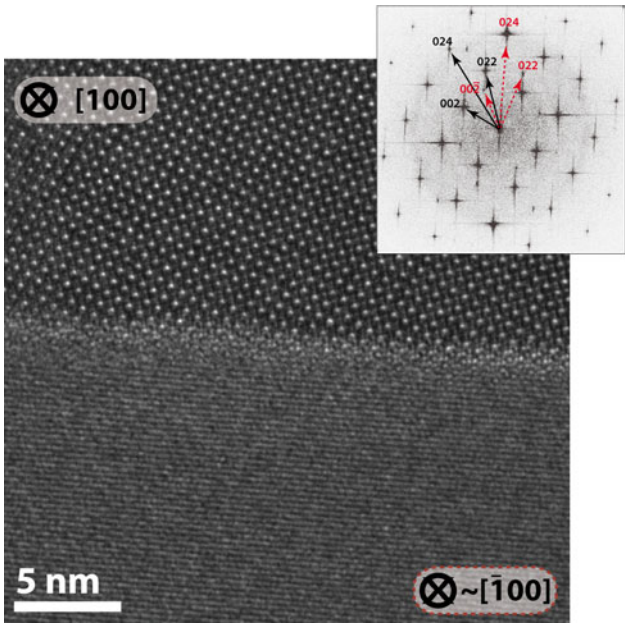

Fig. 3 HRTEM image of the *near* Σ5 (210)/[100] grain boundary. The [100] direction of the upper crystal is parallel to the incident beam. [100] is the common axis of a perfect Σ5 twin boundary. As the misorientation with respect to this orientation is small, both crystals show the diffraction pattern of the [100] zone axis rotated by 36.9°. Nevertheless, the lower crystal is not perfectly aligned in [100]. The TEM-lamella is very thin (see text) and the diffraction spots, with their relatively large deviation vector **s** (**g** = Δ**k** + **s**), are still visible in the diffraction pattern, but with reduced intensities (compare to simulated diffraction pattern in Fig. 1). In the lattice fringe image only the (240) planes of the lower crystal are visible

Table 1 Samples and corresponding bonding conditions

Annealing hours at K							
	673 K	873 K	1,073 K	1,273 K	1,723 K	1,873 K	Separable
2 Garnet	168						Yes
3 Garnet	168	48					Yes
4 Garnet	168		48				Yes
5 Garnet	168			48			No
6 Garnet	168				48		No
7 Garnet	168					48	No
1 Olivine	168						Yes

The primary annealing time was 1 week at 673 K. Additionally, some crystals were annealed for 48 h at varying temperatures. All anneals were done in air. The olivine has previously been synthesized (Heinemann et al. 2005)

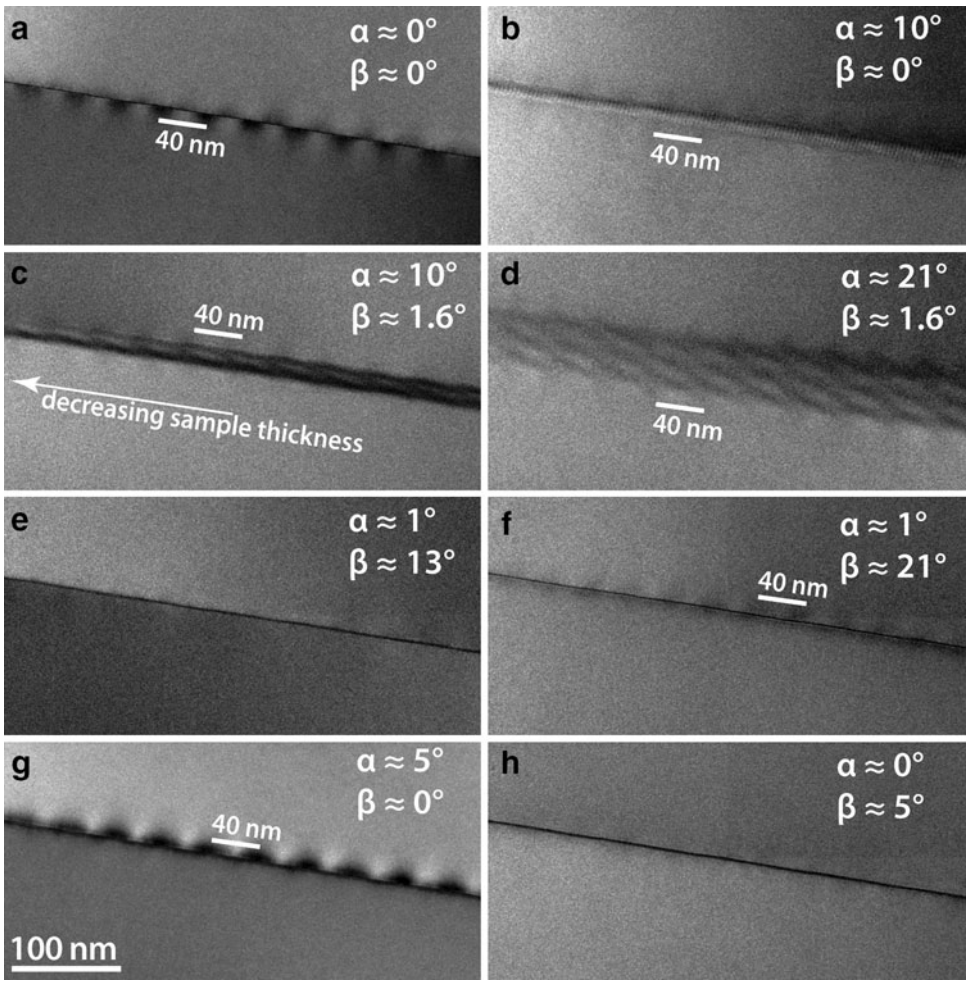

Fig. 4 TEM bright field images of the bicrystal grain boundary. The sample thickness decreases towards the left margin of all the images. **a** The orientation is the same as in Fig. 3 (α and β tilt close to 0°). The periodicity of the dark contrast along the grain boundary is about 40 nm. The distance from a dark contrast maximum in one crystal to a dark contrast maximum in the other crystal is about 20 nm. **b** The same sample, but tilted by $\alpha = 0°$ $\beta = 10°$. The periodicity observed in **a** is still visible, but now interferes with a moiré pattern that is formed by the two superimposed crystal lattices of the bicrystal. To illustrate this effect, the sample is further tilted as shown in '**c**' and '**d**'. **c** The sample is tilted by $\alpha = 10°$ and $\beta = 1.6°$. **d** The sample is tilted by $\alpha = 21°$ and $\beta = 1.6°$. Note that the pattern in '**d**' could be misinterpreted as a network of secondary interface dislocations. **e** The sample is tilted by $\alpha = 1°$ and $\beta = 13°$. The periodic contrast completely disappears. **f** The sample is tilted by $\alpha = 1°$ and $\beta = 21°$. The periodic strain contrast is again visible in both crystals. **g** The sample is tilted by $\alpha = 5°$ and $\beta = 0°$. The periodic strain contrast is visible only in the upper crystal, but very pronounced. **h** The sample is tilted by $\alpha = 0°$ and $\beta = 5°$. The contrast of the extended strain fields is again absent

less than 0.3 the inelastic mean free paths, which was extracted with electron energy loss spectroscopy (EELS) using the Log-Ratio method.

Grain boundary topography

This section describes TEM observations on the 10–100 nm length scale. TEM images and high-resolution images show a long-range periodic diffraction contrast where dark and white contrasts alternate along the grain boundary [Figs. 4, 5; we will henceforth speak of extended strain contrast to use the terms common in literature (Vargas et al. 1997; Tsu et al. 1998)]. The image of the boundary plane is sharp and very narrow indicating that it is edge-on throughout the whole lamella thickness (up to ~80 nm, Fig. 4a). The long-range strain contrast has a periodicity of 40 nm and extends approximately 40 nm into the opposing grains. The periodicity is insensitive to tilting (Fig. 4a–d), whereas, tilting gives rise to an additional moiré pattern, i.e. an interference pattern which is created, in the specific case, by overlaying two grids at an angle. It changes its periodicity depending on the inclination of the boundary plane towards the incident beam (Fig. 4b–d). The moiré pattern interferes with thickness fringes arising from the wedge-shaped projection of the inclined grain boundary plain.

Lattice fringe micrographs reveal steps at the interface. Steps along the grain boundary plane [(042), equivalent to (210)] are observed (Fig. 5a). They extend over at least two

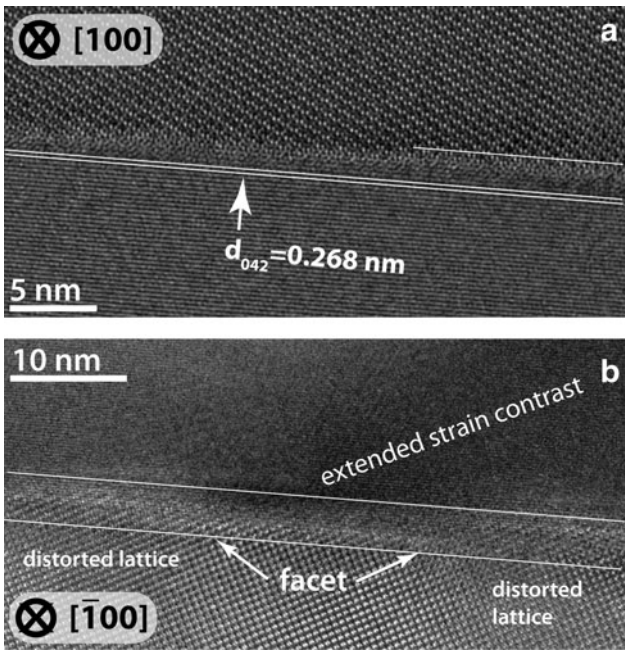

Fig. 5 **a** The same sample as in Fig. 2, but with a different defocus. The actual location is very close to the edge and has relative thickness of less than 0.3 inelastic mean free paths (details above). A step/facet is present along the grain boundary. Lines parallel to the (042) planes, shifted downwards and upwards to prevent coverage of the real structure, are shown for illustration. The step extends over at least two d-spacings of the (042) plane, corresponding to 0.536 nm. **b** Lattice fringe image of the bicrystal at a thicker part of the sample, where the zone axis of the lower crystal is oriented parallel to the incident beam. Most of the grain boundary plane area lies in the (042) plane except for a facet which is spatially related to the extended strain contrast represented by the *dark contrast*. Furthermore, the lattice on both sides of the facet is distorted, causing a slightly blurred image

d-spacings of the (042) plane, corresponding to 0.536 nm. They are of minor height and occur accumulated, thereby forming facets with shallow slopes with a length of about 20 nm. No dislocations were identified. Comparable structures are observed at thicker parts of the sample (Fig. 5b), where most of the grain boundary area lies in the (042) plane, except for some facets. These facets are spatially related to the extended strain contrast (dark contrast in the image). Furthermore, the lattice left and right of the facet structure is distorted, causing a slightly blurred image. The step-high is approx. 1.1 nm (4*d(042)) on the left and approx. 2.1 nm (8*d(042)) on the right site of the facet in Fig. 5. The jump from one platform of the grain boundary plane to the next is indefinite and blurred.

Discussion

Direct bonding— atomic bond formation

In our experiments, the grain boundary in YAG reaches maximum stability only at temperatures T above about 1,273 K, which corresponds to a homologous temperature $T_H = T/T_M$ of 0.58 (the melting temperature T_M of YAG is ~2,213 K). This also holds true for crystalline silicon with a melting temperature of 1,687 K, where complete bonding via surface diffusion of Si atoms occurs above 973 K (Tong and Gösele 1999), which also translates to $T_H = 0.58$. Heinemann et al. (2005) observed using HRTEM that the grain boundary structure in synthetic olivine bicrystals did not differ between annealing temperatures of 673 and 1,923 K. The fact that the olivine bicrystals synthesised at 673 K are mechanically easily separable (as reported in this study) is in good agreement with our observations for YAG. Consequently, we suggest that direct bonded samples should be annealed at temperatures of about 60% of T_m in order to obtain a grain boundary with maximum stability.

Periodic strain fields

A possible relation between the primary surface properties of the educt-materials and the periodic strain fields is evaluated in the following paragraph. Wafers are typically affected by non periodic mm-scale surface morphology (Maszara et al. 1991). Additionally, our wafers had a surface roughness of about 0.34 nm as determined by interferometry. Both surface unevenness deviate from the observed strain field periodicity of 40 nm by several orders of magnitude and do not have any periodicity. A relation between the periodic strain fields and the primary surface properties of the wafers used for direct bonding is thus unlikely. This conclusion is supported by previous studies that report comparable extended periodic strain fields in different materials; the grain boundaries were synthesized by different methods, including direct bonding (Heinemann et al. 2005), directional solidification (Tsu et al. 1998) or they were grown from a flux (Vargas et al. 1997). The wavelengths of the observed periodic strain fields range from 35 to 180 nm. They are not correlated to the misorientation angles as shown for tilt angles ranging from 2° to 31° (Tsu et al. 1998). Tsu et al. (1998) observed a spatial relation between the periodic strain fields and the facets, whereas Heinemann et al. (2005) did not. However, it appears that they are often related to saw-tooth like facet structures (e.g. Tsu et al. 1998; Phaneuf 1999). Nano-scale waviness has also been observed in Olivine (Johnson et al. 2004). All those observations have been obtained from low angle tilt grain boundaries, and have not been reported for perfect or near Σ-orientations (Campbell 1996; Lee et al. 2003b).

Our tilt experiments prove that the measured 40 nm periodicity of the strain contrast (Fig. 4) is an intrinsic property of the grain boundary. The observed contrast pattern in Fig. 4d can be assigned to a rotational moiré

pattern and is not caused by a network of secondary grain boundary dislocations because the horizontal and vertical distances between dark and bright contrast change with sample tilt due to projection. Additionally, the pattern interferes with thickness fringes arising from the wedge-shaped projection of the inclined grain boundary plane. If the contrast of the periodic strain fields is visible depends on the sample orientation relative to the incident electron beam (Fig. 4). During tilting, the imaging vector g and the deviation parameters change, thus modifying the amplitude of the diffracted beam and the direct beam. If dislocations were present, their dislocation line u would be parallel to the imaging vector g in Fig. 4e, h. However, the absence or presence of dislocations is hard to prove because of limitations in the α and β ($\pm 30°$) tilts. In addition, the orientation of our FIB lamella might be unfavourable. It is impossible to follow a Burgers circuit in the HRTEM images, because one crystal is always out of the ideal zone axis. The observed strain fields are large compared to usual dislocation strain fields and it is unlikely that single dislocations account for such large strain fields. Nevertheless, dislocations with delocalized cores, smeared out in the plane of the grain boundary, could cause extended strain fields.

However, steps are directly observed (Fig. 5a, b) in the grain boundary plane area, which mainly lies in the (210) plane. Their heights range from $\sim$0.5 to $\sim$2.1 nm, which are multiples of d(042) = 0.268 nm. They correlate spatially with the periodic contrast of the extended strain fields (Fig. 5b). The association between steps and strain contrast becomes only visible in thicker parts of the sample (Fig. 5b), whereas the strain contrast decreases drastically as the sample thickness drops below a thickness of about one extinction length (Fig. 5a). The change in contrast formation with decreasing sample thickness can be described applying the dynamical theory in thicker parts of the lamella and the kinematic theory for contrast formation in very thin parts. The central point is that as the sample thickness decreases the jump from one platform of the grain boundary plane to the next is much sharper. Hence, a component of the facet structure extends in the third dimension and could be responsible for the extended strain fields. The facet structure could also include dislocations, discontinuities or disconnections to a small extend in the plane of the boundary (Pond 1989; Lartigue-Korinek et al. 2008). But as the additional misfit is tilt in character we would expect them to be mainly out of the plane of the grain boundary. Using two beam imaging with the {240} coincidence diffraction spots, we did not detect dislocations with a Burgers vector belonging to the CSL.

The facets seem to generate a wavy interface (Figs. 4e, h, 5b), similar to a low amplitude saw-tooth structure. The observed facets and the orientation of the grain boundary plane strengthen the argument that small misorientations of the grain boundary plane relative to a low Σ-plane orientation are adjusted by inserting steps, which is energetically favoured over facet-free boundaries with random grain boundary plane orientations. A superimposed dislocation network, during relaxation, could then accommodate the stress generated by the overall misorientation.

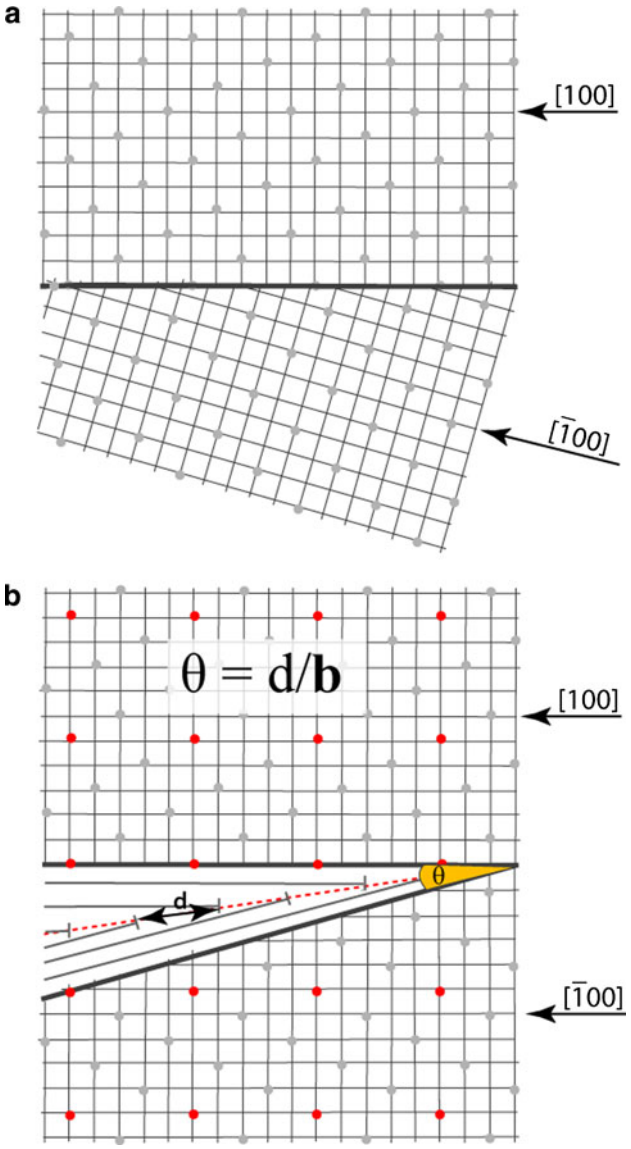

Fig. 6 **a** The tilting which is needed to turn a near Σ-crystal orientation to a low Σ-orientation can be achieved by introducing dislocations similar to those of a low angle boundary to the present boundary. **b** The additional misorientation angle for small angles is given by θ = d/**b** with dislocations spacing of the DSC lattice d, and the Burgers vector of the DSC lattice dislocations **b**. The dislocations in **b** could be distributed between the lower and the upper crystal, thereby generating a smoothly waved interface. The different contrasts that we observe for the two crystals in our experimental TEM images are caused by the fact that the atom columns of the upper crystal are parallel to the incident beam, whereas the atom columns of the lower crystal are not

Based on theoretical considerations (e.g. Brandon 1966), a bicrystal with an orientation relation close to a Σ-orientation should decrease its total free energy by introducing grain boundary dislocations with a Burgers vector of the DSC lattice that belongs to the Σ-orientation. The dislocation-free parts would then be in Σ-orientation and the mismatch would be compensated by the grain boundary dislocations (sketch in Fig. 6). In our case, the $[\bar{1}00]$ zone axis should then be tilted parallel to the [100] of the second crystal; necessarily the grain boundary dislocations must than have a Burgers vector b perpendicular to the boundary plane. However, this was not observed. Similarly, Randle et al. (2008) used electron backscattering diffraction (EBSD) and observed subtle changes in the plane distribution as a consequence of a long low temperature anneal in hexagonal titanium alloy, but the pure CSL relation also stayed nearly unchanged. Further studies are needed to find out if the pure CSL relation can change at all.

Conclusion

For the first time, periodic extended strain fields in relation with a *near* Σ grain boundary have been observed. They are an intrinsic property of the grain boundary. We interpret them to arise from facets at the grain boundary plane, which compensate a slight off-plane component of the (210) grain boundary plane. Another interpretation is that the bicrystal started to adjust for its off-Σ relation by introducing secondary grain boundary dislocations in order to compensate the misfit rotation of $\theta \sim 6.5°$ about the [210] direction.

This well characterized grain boundary provides an excellent starting material for further studies, for example diffusion experiments along single grain boundaries (Hartmann et al. 2008 and Hartmann et al. in preparation).

Acknowledgments The authors would like to thank FEI Company in Eindhoven for preparing a FIB sample which was used for the HREM image of Fig. 3 as well as for Figs. 4 and 5. We thank Carl ZEISS NTS GmbH in Oberkochen, Germany, for sample preparation with low energy Ar-ion polishing. Furthermore, KH highly appreciates the hours of in-depth discussion with Hauke Marquardt and likes to thank him for his critical opinion of the manuscript.

References

Abart R, Kunze K, Milke R, Sperb R, Heinrich W (2004) Silicon and oxygen self diffusion in enstatite polycrystals; the Milke et al. (2001) rim growth experiments revisited. Contrib Miner Petrol 147:633–646

Abart R, Petrishcheva E, Fischer FD, Svoboda J (2009) Thermodynamic model for diffusion controlled reaction rim growth in a binary system; application to the forsterite-enstatite-quartz system. Am J Sci 309:114–131

Bons AJ, Drury MR, Schryvers D, Zwart HJ (1990) The nature of grain boundaries in slates; implications for mass transport processes during low temperature metamorphism. Phys Chem Miner 17:402–408

Brandon DG (1966) The structure of high-angle grain boundaries. Acta Metall 14:1479–1484

Campbell GH (1996) Σ5 (210)/[001] Symmetric tilt grain boundary in yttrium aluminum garnet. J Am Ceram Soc 79:2883–2891

Carter CB, Föll H (1978) The contrast from incoherent twin interfaces observed using the weak-beam technique. Scr Metall 12:1135–1139

Carter CB, Föll H, Ast DG, Sass SL (1981) Electron diffraction and microscopy studies of the structure of grain boundaries in silicon. Philos Mag A 43:441–467

Caslavsky JL, Viechnicki DJ (1980) Melting behaviour and metastability of yttrium aluminium garnet (YAG) and YAlO3 determined by optical differential thermal analysis. J Mater Sci 15:1709–1718

Chadwick GA, Smith DA (1976) Grain boundary structure and properties. Academic, London

Christophersen M, Carstensen J, Rönnebeck S, Jäger C, Jäger W, Föll H (2001) Crystal orientation dependence and anisotropic properties of macropore formation of p- and n-type silicon. J Electrochem Soc 148:E267–E275

Cunningham B, Strunk HP, Ast DG (1982) High resolution electron microscopy of a $\Sigma = 27$ boundary in silicon. Scr Metall 16:349–352

Dobrzycki L, Bulska E, Pawlak DA, Frukacz Z, Wozniak K (2004) Structure of YAG crystals doped/substituted with erbium and ytterbium. Inorg Chem 43:7656–7664

Ernst F, Kienzle O, Rühle M (1999) Structure and composition of grain boundaries in ceramics. J Eur Ceram Soc 19:665–673

Föll H, Ast D (1979) TEM observations on grain boundaries in sintered silicon. Philos Mag A 40:589–610

Gemming T, Nufer S, Kurtz W, Ruhle M (2003) Structure and chemistry of symmetrical tilt grain boundaries in α-Al_2O_3: I, bicrystals with "clean" interface. J Am Ceram Soc 86:581–589

Gleiter H, Chalmers B (1972) High-angle grain boundaries. Pergamon, Oxford

Gösele U, Tong QY, Schumacher A, Kräuter G, Reiche M, Plößl A, Kopperschmidt P, Lee TH, Kim WJ (1999) Wafer bonding for microsystems technologies. Sens Actuators A Phys 74:161–168

Haisma J, Spierings BACM, Biermann UKP, van Gorkum AA (1994) Diversity and feasibility of direct bonding: a survey of a dedicated optical technology. Appl Opt 33:1154–1168

Harendt C, Graf H-G, Höfflinger B, Penteker E (1992) Silicon fusion bonding and its characterization. J Micromech Microeng 2:113–116

Hartmann K, Wirth R, Dohmen R, Dresen G, Heinrich W (2008) Diffusion in synthetic grain boundaries. In: Richter S, Schwedt A (eds) EMC 2008 materials science. Springer, Berlin, pp 817–818

Heinemann S, Wirth R, Dresen G (2001) Synthesis of feldspar bicrystals by direct bonding. Phys Chem Miner 28:685–692

Heinemann S, Wirth R, Dresen G (2003) TEM study of a special grain boundary in a synthetic K-feldspar bicrystal: Manebach twin. Phys Chem Miner 30:125–130

Heinemann S, Wirth R, Gottschalk M, Dresen G (2005) Synthetic [100] tilt grain boundaries in forsterite: 9.9 to 21.5°. Phys. Chem. Miner 32:229

Jaoul O, Sautter V, Abel F (1991) Nuclear microanalysis; a powerful tool for measuring low atomic diffusivity with mineralogical applications. Adv Phys Geochem 8:198–220

Joesten R (1991) Grain-boundary diffusion kinetics in silicate and oxide minerals, Diffusion, atomic ordering, and mass transport; selected topics in geochemistry. Springer, New York, pp 345–395

Johnson CL, Hÿtch MJ, Buseck PR (2004) Nanoscale waviness of low-angle grain boundaries. Proc Natl Acad Sci USA 101:17936–17939

Keller LM, Wirth R, Rhede D, Kunze K, Abart R (2008) Asymmetrically zoned reaction rims: assessment of grain boundary diffusivities and growth rates related to natural diffusion-controlled mineral reactions. J Met Geol 26:99–120

Kim MJ, Carpenter RW (2002) Heterogeneous silicon integration by ultra-high vacuum wafer bonding. In: 3rd international conference on alternative substrate technology (ICAST), pp 849–854

Kuklja MM, Pandey R (1999) Atomistic modeling of native point defects in yttrium aluminum garnet crystals. J Am Ceram Soc 82:2881–2886

Lartigue-Korinek S, Liagege S, Kisielowski C, Serra A (2008) Disconnection arrays in a rhombohedral twin in alpha-alumina. Philos Mag 88:1569–1579

Lee MR, Bland PA, Graham G (2003a) Preparation of TEM samples by focused ion beam (FIB) techniques; applications to the study of clays and phyllosilicates in meteorites. Mineral Mag 67:581–592

Lee SB, Sigle W, Kurtz W, Rühle M (2003b) Temperature dependence of faceting in Σ5(310)[001] grain boundary of $SrTiO_3$. Acta Mater 51:975–981

Maszara WP (1991) Silicon-on-insulator by wafer bonding—a review. J Electrochem Soc 138:341–347

Maszara WP, Jiang BL, Yamada A, Rozgonyi GA, Baumgart H, Dekock AJR (1991) Role of surface-morphology in wafer bonding. J Appl Phys 69:257–260

Merkle KL, Thompson LJ, Phillipp F (2004) In situ HREM Studies of Grain Boundry Migration. Interface Sci 12:277–292

Milke R, Abart R, Kunze K, Koch M, Ller M, Schmid D, Ulmer P (2009) Matrix rheology effects on reaction rim growth I: evidence from orthopyroxene rim growth experiments. J Met Geol 27:71–82

Overwijk MHF, van den Heuvel FC, Bulle-Lieuwma CWT (1993) Novel scheme for the preparation of transmission electron microscopy specimens with a focused ion beam. J Vac Sci Technol B 11:2021–2024

Phaneuf MW (1999) Applications of focused ion beam microscopy to materials science specimens. Micron 30:277–288

Pond RC (1989) Line defects in interfaces. In: Nabarro FRN (ed) Dislocations in solids. Elsevier, Amsterdam, pp 1–66

Pößl A, Kräuter G (1999): Wafer direct bonding: tailoring adhesion between brittle materials. Materials Science and Engineering. Reports: 1–88

Pradère P, Thomas EL (1990) Image processing of partially periodic lattice images of polymers: the study of crystal defects. Ultramicroscopy 32:149–167

Pradère P, Revol JF, Nguyen L, St. John Manley R (1988) Lattice imaging of poly-4-methyl-pentene-1 single crystals; use and misuse of fourier averaging techniques. Ultramicroscopy 25:69–80

Randle V, Rohrer GS, Hu Y (2008) Five-parameter grain boundary analysis of a titanium alloy before and after low-temperature annealing. Scr Mater 58:183–186

Razek N, Schindler A, Rauschenbach B (2007) Ultra-high vacuum direct bonding of a p-n junction GaAs wafer using low-energy hydrogen ion beam surface cleaning. Vacuum 81:974–978

Rohrer GS (2007) The distribution of grain boundary planes in polycrystals. JOM 59:38–42

Rohrer GS, El Dasher BS, Miller HM, Rollett AD, Saylor DM (2004) Distribution of grain boundary planes at coincident site lattice misorientations. Materials Research Society N7.2

Schmid DW, Abart R, Podladchikov YY, Milke R (2009) Matrix rheology effects on reaction rim growth II: coupled diffusion and creep model. J Met Geol 27:83–91

Sutton AP, Balluffi RW (1995) Interfaces in crystalline materials. Clarendon, Oxford

Tong QY, Gösele U (1999) Semiconductor wafer bonding: science and technology. Wiley, New York

Tong QY, Gösele U, Martini T, Reiche M (1995) Ultrathin single-crystalline silicon on quartz (SOQ) by 150°C wafer bonding. Sens Actuators A 48:117–123

Tsu IF, Wang J-L, Kaiser DL, Babcock SE (1998) A comparison of grain boundary topography and dislocation network structure in bulk-scale [001] tilt bicrystals of $Bi_2Sr_2CaCu_2O_{8+x}$ and $YBa_2Cu_3O_{7-\delta}$. Phys C Supercond 306:163–187

Vargas JL, Zhang N, Kaiser DL, Babcock SE (1997) Systematic copper concentration variations along grain boundaries in bulk-scale $YBa_2Cu_30_{7-\delta}$ bicrystals. Phys C Supercond 292:1–16

Wirth R (2004) Focused ion beam (FIB): a novel technology for advanced application of micro- and nanoanalysis in geosciences and applied mineralogy. Eur J Mineral 16:863–876